

Performance evaluation of the Alphasense OPC-N3 and Plantower PMS5003 sensor in measuring dust events in the Salt Lake Valley, Utah

Kamaljeet Kaur¹, Kerry E. Kelly¹

¹Department of Chemical Engineering, University of Utah, SLC, 84102, USA

Correspondence to: Kerry Kelly (kerry.kelly@utah.edu)

Abstract. As the changing climate expands the extent of arid and semi-arid lands, the number, severity of, and health effects associated with dust events are likely to increase. However, regulatory measurements capable of capturing dust (PM₁₀, particulate matter smaller than 10 µm in diameter) are sparse, sparser than measurements of PM_{2.5} (PM smaller than 2.5 µm in diameter). Although low-cost sensors could supplement regulatory monitors, as numerous studies have shown for PM_{2.5} concentration, most of these sensors are not effective at measuring PM₁₀ despite claims by sensor manufacturers. This study focuses on the Salt Lake Valley, adjacent to the Great Salt Lake, which recently reached historic lows exposing 1865 km² of dry lakebed. It evaluated the field performance of the Plantower PMS 5003, a common low-cost PM sensor, and the Alphasense OPC-N3, a promising candidate for low-cost measurement of PM₁₀, against a federal equivalent method (FEM, beta attenuation) and research measurements (GRIMM aerosol spectrometer model 1.109) at three different locations. During a month-long field study that included five dust events in the Salt Lake Valley with PM₁₀ concentrations reaching 311 µg/m³, the OPC-N3 exhibited strong correlation with FEM PM₁₀ measurements ($R^2 = 0.865$, RMSE = 12.4 µg/m³) and GRIMM ($R^2 = 0.937$, RMSE = 17.7 µg/m³). The PMS sensor exhibited poor to moderate correlations ($R^2 < 0.49$, RMSE = 33-45 µg/m³) with reference/research monitors and severely underestimated the PM₁₀ concentrations (slope < 0.099) for PM₁₀. We also evaluated a PM-ratio-based correction method to improve the estimated PM₁₀ concentration from PMS sensors. After applying this method, PMS PM₁₀ concentrations correlated reasonably well with FEM measurements ($R^2 > 0.63$) and GRIMM measurements ($R^2 > 0.76$), and the RMSE decreased to 15-25 µg/m³. Our results suggest that it may be possible to obtain better resolved spatial estimates of PM₁₀ concentration using a combination of PMS sensors (often publicly available in communities) and measurements of PM_{2.5} and PM₁₀, such as those provided by FEMs, research-grade instrumentation, or the OPC-N3.

1 Introduction

Our changing climate is expanding the extent of arid and semi-arid lands globally; these lands currently cover approximately 1/3rd of the Earth's land surface (Williams et al., 2022; Huang et al., 2016). Recent studies suggest that this expansion of arid lands is linked to increases in the number and severity of dust events (Clifford et al., 2019; Tong et al., 2017; Ardon-Dryer and Kelley, 2022). Dust events can transport particulate matter (PM), particle-bound air toxics, and allergens over thousands of kilometers (Goudie, 2014). The suspended PM affects regional climate by

33 impacting cloud formation, precipitation processes, and convection activity (Cai et al., 2021; Kumar et al., 2021;
34 Mallet et al., 2009). Dust events significantly affect the regional air quality (Chakravarty et al., 2021; Akinwumiju et
35 al., 2021; Liu et al., 2020), decrease atmospheric visibility (Jayaratne et al., 2011) and have adverse effects on human
36 health, including being linked to increased incidence of asthma, pneumonia, bronchitis, stroke, adverse birth outcomes,
37 influenza, meningitis, and valley fever (Dastoorpoor et al., 2018; Jones, 2020; Bogan et al., 2021; Soy, 2016; Trianti
38 et al., 2017; Diokhane et al., 2016; Schweitzer et al., 2018).

39

40 During dust events, the majority of PM is greater than 2.5 μm in diameter (Tam et al., 2012). Government
41 organizations, such as the World Health Organization (WHO), measure and/or provide guidelines for ambient PM₁₀
42 concentrations (PM₁₀, particles with aerodynamic diameter <10 μm). PM smaller than 10 μm in diameter is of
43 particular interest because it is inhalable. The WHO has set guidelines for 24-hour and annual average PM₁₀
44 concentration at 45 and 15 $\mu\text{g}/\text{m}^3$, respectively (WHO, 2022). The US EPA's national ambient air quality standard for
45 PM₁₀ concentration and are 150 and 50 $\mu\text{g}/\text{m}^3$ for the 24-hour and annual average, respectively. One challenge with
46 24-hour standards/guidelines is that dust events often last a few hours, and these events are obscured when reporting
47 only the PM₁₀ 24-hour average or comparing these averages to the 24-hour guidelines (Ardon-Dryer and Kelley,
48 2022).

49

50 PM₁₀ concentrations tend to be more spatially heterogenous than PM_{2.5} concentrations because PM₁₀ settles more
51 quickly (Keet et al., 2018). In addition, regulatory measurements of PM₁₀ are spatially and temporally sparser than
52 PM_{2.5} measurements. For example, the US EPA reports measurements from 1,370 active PM_{2.5} sites versus 800 active
53 PM₁₀ sites (EPA, 2022). Approximately half of these PM₁₀ sites only report 24-hour averages (USA EPA, 2022).
54 Furthermore, many dust-prone areas of the US lack any PM monitoring (USA EPA, 2022). More highly resolved
55 measurements of PM₁₀ concentration would aid communities and researchers in understanding and addressing the
56 effects of windblown dust and dust events.

57

58 More recent studies of PM have leveraged low-cost PM measurements and mobile measurements to obtain higher
59 spatial and temporal resolution PM_{2.5} estimates (Bi et al., 2020; Caplin et al., 2019; Lim et al., 2019; Caubel et al.,
60 2019; Kelly et al., 2021). With appropriate calibration, low-cost sensors have been demonstrated to be generally
61 effective at measuring PM_{2.5}; however, the most common low-cost PM sensors that employ a laser, and a photodiode
62 to estimate particle concentration (Plantower PMS, Nova SDSS011, Sensirion SPS30, Shineyi PPD42NS, and
63 Samyoung DSM501A) are ineffective at measuring PM₁₀ and dust (Kosmopoulos et al., 2020; Mei et al., 2020; Sayahi
64 et al., 2019, Kuula et al. 2020) primarily due to truncation of the forward scattering coefficient for larger particles and
65 in potentially due to the sensors' inability to aspirate the larger particles into the device (Ouimette et al., 2022). Kuula
66 et al. (2020) tested several low-cost PM sensors using monodisperse di-octyl sebacate particles (0.5 – 10 μm) and
67 observed a constant particle size distribution for particle sizes >0.5 μm and indicated that these sensors are incapable
68 of measuring coarse-mode particles (2.5-10 μm).

69

70 The Alphasense OPC-N series is a promising low-cost sensor for measuring PM₁₀. It is larger and more expensive
71 (~\$500) than many of the low-cost PM sensors (<\$50) with a greater flow rate (total flow of 5.5 LPM and sample
72 flow rate of 0.28 L/min) and a mirror that allows collection of light scattering from broader array of angles than typical
73 low-cost PM sensors, which have flow rates on the order of 0.1 LPM (Sayahi et al., 2019; Ouimette et al., 2022;
74 Alphasense Ltd, 2022). The OPC-N3 allows particle counting in 24-size bins for sizes ranging from 0.35-40 μm. The
75 working principle of Alphasense OPC-N3 and its previous version (OPC-N2) is similar to an aerosol spectrometer; it
76 measures scattering from single particles (Vogt et al., 2021). Studies have used the Alphasense OPCs for indoor and
77 ambient PM monitoring (Kaliszewski et al., 2020; Chu et al., 2021; Dubey et al., 2022b; Feenstra et al., 2019; Pope
78 et al., 2018; Nor et al., 2021; Alhasa et al., 2018; Mohd Nadzir et al., 2020), to monitor PM_{2.5} personal exposure (Harr
79 et al., 2022a), to identify PM sources (Harr et al., 2022b; Bousiotis et al., 2021), and to monitor occupational PM_{2.5}
80 and PM₁₀ exposure (Runström Eden et al., 2022; Bächler et al., 2020). The Alphasense OPCs correlate well ($R^2 =$
81 0.93-0.99) with PM₁₀ in laboratory studies (Sousan et al., 2021, 2016; Samad et al., 2021; Dubey et al., 2022a). The
82 field-based studies have reported somewhat lower correlations (R^2 : 0.53 – 0.8) (Bílek et al., 2021; Dubey et al., 2022b,
83 a; Crilley et al., 2018), due to the variable ambient meteorological conditions and changing PM compositions. The
84 ambient PM ratios (PM_{2.5}/PM₁₀) in these previous studies were greater than 0.6, indicating the main contributions to
85 PM levels were from the fine PMs, rather than coarser PMs. The ratio of PM_{2.5}/PM₁₀ can provide crucial information
86 about particle origin and formation process (Xu et al., 2017; Speranza et al., 2014). Duvall et al. (2021) have suggested
87 evaluating the performance of PM₁₀ sensors for varying PM_{2.5}/PM₁₀ ratios, and dust events provide a great opportunity
88 to evaluate PM₁₀ sensor performance at ambient PM ratios <0.3.

89
90 Few studies have evaluated the performance of Alphasense OPCs for measuring PM₁₀ concentration during dust
91 events. Gomes et al. (2022) measured hourly PM₁₀ concentration exceeding 300 μg/m³ using the OPC-N3 during
92 Saharan dust events in western Portugal. In Sarajevo, Bosnia-Herzegovina, Masic, et al. (2020) reported that for the
93 Aralkum Desert dust event, the OPC-N2 tracked GRIMM-11D PM₁₀ measurements but at a lower magnitude. Fewer
94 studies have compared the Alphasense OPCs with the regulatory monitors during dust events. Vogt et al. (2021)
95 reported that the OPC-N3 captures the long-range transported dust well, but slightly overestimates PM₁₀ concentration
96 (<120 μg/m³) compared to a FIDAS (EN 16450 approved regulatory instrument). They also reported a moderate
97 correlation with PM₁₀ compared to FIDAS ($R^2 = 0.58-0.64$, and RMSE between 12-13 μg/m³) and compared to a
98 gravimetric method ($R^2 = 0.71-0.74$, and RMSE between 9-11 μg/m³). Mukherjee et al. (2017) evaluated the OPC-N2
99 performance against a Met One beta attenuation monitor (BAM) over 12 weeks in the Cuyama Valley of California,
100 where PM concentrations are impacted by wind-blown dust events and regional transport; they reported a moderate
101 to good degree of correlation ($R^2 = 0.53-0.81$, depending on sampling orientation) for PM₁₀ (<750 μg/m³). In general,
102 the studies report that the OPC-N2/N3 tracks the temporal variation of research/reference measurements but with
103 varying correlation factors.

104
105 A high PM_{2.5}/PM₁₀ ratio represents fine-dominated aerosols, likely corresponding to anthropogenic or other
106 combustion sources. Low ratios represent coarser particles (aerodynamic size between 2.5-10 μm) that tend to

107 correspond to wind-blown dust (Sugimoto et al., 2016). Sugimoto et al. (2016) classified aerosols as local dust when
108 the $PM_{2.5}/PM_{10}$ ratio was less than 0.1 and as transported dust when $PM_{2.5}/PM_{10}$ ratios were between 0.1 to 0.3. During
109 dust events, low-cost sensors like the Plantower PMSs can detect only a small portion of a particle size distribution,
110 and its response greatly depends on the particle size distribution and particle optical properties (Vogt et al., 2021).
111 This study explores the possibility of using a size-segregated correction factor ($PM_{2.5}/PM_{10}$ ratio) to infer PM_{10}
112 concentration from low-cost sensors that typically respond poorly to particles larger than 2.5 μm in diameter. If
113 successful, this technique could leverage the large number of existing low-cost sensor measurements that use the
114 Plantower PMS (and similar sensors) and improve spatial estimates of PM_{10} concentration.

115

116 This study aims to evaluate the Alphasense OPC-N3 to complement common low-cost PM measurements to
117 understand PM_{10} concentrations during dust events in the Salt Lake Valley. The Salt Lake Valley is particularly well
118 suited to studying dust events because it is affected by both regional dust events from the playas located to the west
119 of the valley and from the drying Great Salt Lake bed, which has reached historic lows with more than 1865 km^2 of
120 exposed lakebed (Perry et al., 2019). Under appropriate meteorological conditions, portions of this exposed lakebed
121 produce substantial dust plumes, and the winds can transport this dust directly into the populated areas of the Salt
122 Lake Valley (Perry et al., 2019).

123

124 **2 Methods**

125 This study focused on April of 2022 in the Salt Lake Valley, when it experienced five dust events (summarized in
126 Table 1). It relies on low-cost sensors and reference/research measurements at three different locations (Fig. 1): the
127 Utah Division of Air Quality (UDAQ)'s Hawthorne monitoring station (HW), the UDAQ's Environmental Quality
128 (EQ) station and surroundings, and a residential site (RS) in the northeast quadrant of the Salt Lake Valley. This period
129 included an hourly average FEM (Federal Equivalent Method) PM_{10} concentration that reached 311 $\mu g/m^3$.



130
 131
 132
 133
 134
 135
 136
 137
 138
 139
 140
 141
 142
 143
 144
 145
 146
 147
 148
 149
 150
 151

Figure 1: Study locations in Salt Lake County: EQ (UDAQ Environmental Quality) site, HW (Hawthorne UDAQ) site, and RS (residential site). The distance between EQ to HW, HW to RS, and EQ to RS is 7.8 km, 4.3 km, and 7.35 km, respectively. The OPC and PMS sensors were collocated at RS and HW sites. Two PurpleAir II were located within 2 km of the EQ monitoring station.

152 **Table 1:** PM measurements at the three different study locations.

153

Site	Measurement type	Working principle	#	Sensor ID	Distance from a reference monitor	Hours of operation*
HW	OPC-N3	Light Scattering (optical particle counter)	1	OPC-HW	Collocation	633 ^a
	PurpleAir II	Light Scattering- (nephelometry)	2	PMS-HW-1A, PMS-HW-1B, PMS-HW-2A, PMS-HW-2B	Collocation	697
	Thermo Scientific Model 5030 SHARP analyzer	Light scattering (nephelometry) + BAM	1	PM _{2.5} FEM-HW	Federal equivalent method	697
	MetOne E-BAM PLUS	BAM	1	PM ₁₀ FEM-HW	Federal equivalent method	695
EQ	PurpleAir II	Light Scattering- (nephelometry)	2	PMS-EQ-1A, PMS-EQ-1B, PMS-EQ-2A, PMS-EQ-2B	480 m and 1.82 km	697
	Thermo Scientific Model 5030 SHARP analyzer	Light scattering (nephelometry) + BAM		PM _{2.5} FEM-EQ	Federal equivalent method	697
	MetOne E-BAM PLUS	BAM		PM ₁₀ FEM-EQ	Federal equivalent method	697
RS	OPC-N3	Light Scattering (optical particle counter)	1	OPC-RS	Collocation	425 ^c
	PurpleAir II	Light Scattering- (nephelometry)	2	PMS-RS-1A, PMS-RS-1B, PMS-RS-2A, PMS-RS-2B	Collocation	302 ^d
	GRIMM 1.109	Light Scattering (optical particle counter)		GRIMM	Research monitor	452

154 *Total number of available hours = 711. Measurements between 4/11/2022 8:00 pm – 4/12/22 5:00 am were not
 155 available for HW, and subsequently removed for all sensors. Measurements corresponding to relative humidity
 156 >85%, i.e., 14 hrs, were excluded.

157 ^aOPC-HW measurements were not available between 4/12/2022 6:00 pm – 4/14/2022 7:00 pm due to connectivity
 158 issues.

159 ^cThe measurements for OPC-RS were available starting 9 April 2022. OPC-RS measurements between 4/14/2022
 160 10:00 am – 4/17/2022 20:00 pm were not available due to connectivity issues.

161 ^dThe measurements from all the PurpleAir II at RS were available starting on 18 April 2022

162 **2.1 Low-cost sensors**

163 The low-cost sensors tested in this study include the Alphasense optical particle counter (OPC-N3, Alphasense Ltd,
164 \$500) and the Plantower PMS5003 (\$20) integrated into the PurpleAir II (~\$259). The Alphasense OPC-N3 uses a
165 class 1 laser (~658 nm) to detect, size, and count particles in the size range 0.35-40 μm in 24 bins, which is translated,
166 using the embedded algorithm, into estimated PM_{10} , $\text{PM}_{2.5}$, and PM_1 mass concentrations. The default setting for the
167 OPC-N3's refractive index is 1.5 (real part) and for density is 1.65 g/cm^3 , and these default settings were used
168 throughout this study. The OPC-N3 uses an internal fan to create flow and reports a sample flow rate (~0.28 L/min
169 and a total flow rate of 5.5 LPM). Each OPC-N3 was connected to a laptop and used the manufacturer-provided
170 software. The OPC-N3 was set to store measurements every 1 min. The measurements included the date, size bins
171 and counts, pump flow, relative humidity (RH), temperature, and PM_1 , $\text{PM}_{2.5}$, and PM_{10} concentration.

172

173 The PMS 5003 is a low-cost sensor (~\$20, Plantower Technology, China), which has been integrated into a variety of
174 low-cost air quality sensor packages, such as TSI BlueSky, PurpleAir, etc. It uses a fan to create a flow (~0.1 L/min),
175 and it is equipped with a red laser (~680 \pm 10 nm), a scattering angle of 90°, and a photo-diode detector to convert the
176 scattered light to a voltage pulse (Sayahi et al., 2019; Ouimette et al. 2022). The PMS sensor converts light scattering
177 into several different air quality parameters, including particle counts (0.3-10 μm), PM_1 , $\text{PM}_{2.5}$, and PM_{10} , although
178 these different metrics are all based on this single measurement, total light scattering. The PMS 5003 has been
179 evaluated extensively in the laboratory and the field, and the measurements tend to correlate well with PM_1 or $\text{PM}_{2.5}$
180 concentration although it performs poorly for larger PM sizes, such as $\text{PM}_{2.5}$ - PM_{10} (Sayahi et al., 2019; Vogt et al.,
181 2021; Kuula et al., 2020; Ouimette et al., 2022). In this study, we used two PurpleAir PA-II at the HW and RS sites,
182 each PA-II has two PMS sensors per node. PM_{10} mass concentration corresponding to correction factor (CF) =1 and
183 a data collection rate of every 2 minutes were used. The data were downloaded from the PurpleAir website. In addition,
184 we evaluated two PurpleAir PA-II sensors located within 2 km of the EQ monitoring station.

185 All the OPC-N3 were placed inside a custom build housing to protect the sensor from rain and insects. The details of
186 housing can be found in the supplementary material (Section S3).

187

188 **2.2 Site descriptions**

189 The study includes measurements from the two UDAQ sites (HW and EQ) in Salt Lake County that provide both
190 hourly $\text{PM}_{2.5}$ and PM_{10} measurements (Fig. 1). UDAQ uses a Thermo Scientific Model 5030 SHARP analyzer for
191 measuring hourly $\text{PM}_{2.5}$ concentration and a MetOne E-BAM (Beta Attenuation Monitoring) PLUS for measuring
192 PM_{10} concentration. We placed two PurpleAir PA-II (containing four Plantower PMS 5003s, named: PMS-HW-1A,
193 PMS-HW-1B, PMS-HW-2A, PMS-HW-2B) and one OPC-N3 (named: OPC-HW) at the HW site (Table 1). The
194 PurpleAir PA-IIs and the OPC-N3 were mounted on poles that extend above the roof of the HW monitoring station.
195 The HW monitoring station is located in an urban residential area (AQS: 49-035-3006, Lat: 40.7343, Long: -111.8721)
196 at an elevation of 1308m. This site was established to represent population exposure in the Salt Lake City area, and it
197 is often the controlling monitor for the county. The average of PMS-HW-1A, PMS-HW-2A, and PMS-HW-2B PM_{10}

198 concentrations at HW were named PMS-HW. PMS-HW-2B was excluded from the PMS-HW average because of its
199 moderate correlation with the other three sensors (Fig. S2).

200
201 We also evaluated two PurpleAir II (containing four Plantower PMS 5003s, named PMS-EQ-1A, PMS-EQ-1B, PMS-
202 EQ-2A, PMS-EQ-2B) sensors located near the UDAQ EQ site. One of the sensors was 480 m away (PMS-EQ-1),
203 while the other was 1.82 km away (PMS-EQ-2). The EQ monitoring station (AQS: 49-035-3015, Lat: 40.777028,
204 Long: -111.94585, elevation 1284 m) is located approximately 14 km southeast of the Great Salt Lake dry lake bed.
205 In addition to PM concentrations, we accessed relative humidity (RH), temperature, wind speed, and wind direction
206 data from the two UDAQ monitoring sites on EPA's AirNow Tech website. EPA-flagged measurements were
207 excluded from this study. UDAQ uses RM Young Ultrasonic Anemometer Model 86004 to measure the wind speed
208 and wind direction and an instrument based on a hygroscopic plastic film to measure relative humidity.

209
210 The RS was located in the northeast quadrant of the Salt Lake Valley at an elevation of 1383 m (40.771938, -
211 111.861290). Measurements at this site included four Plantower PMS 5003s (labeled as PMS-RS-1A, PMS-RS1B,
212 PMS-RS-2A, PMS-RS-2B) in two PurpleAir PA-IIs, one OPC-N3 (labeled as OPC-RS) and one GRIMM (model
213 1.109 Aerosol Technik Ainring, Germany). The GRIMM employs an internal pump to create a flow of 1.2 L/min and
214 measures the number concentration of particles of size 0.265 μm – 34 μm in 31 size bins, and reports estimated PM₁,
215 PM_{2.5}, and PM₁₀ concentrations. The GRIMM measurements were stored every minute in an internal storage card.
216 The GRIMM measurements were not available between 4/24/2022 6:00PM -4/26/2022 2:00 PM MDT (Mountain Day
217 Time). The PurpleAir PA-IIs and the GRIMM were mounted on the east side of a small outbuilding.

218

219 **2.3 Data Analysis**

220 The measurements from the low-cost sensors and the research monitor (GRIMM) were converted to hourly average
221 concentrations and time-synchronized to MDT. Two EPA-flagged measurements corresponding to unexplainable high
222 hourly PM₁₀ concentrations ($>800 \mu\text{g}/\text{m}^3$) from FEM-HW were removed. The low-cost sensors used in this study were
223 not supplemented with dryers, and therefore their performance is affected by high humidity conditions, which can
224 result in condensation and droplet formation (Samad et al., 2021). Consequently, the measurements corresponding to
225 relative humidity greater than 85% were excluded from the study ($<2\%$ of total measurements).

226

227 Using the HW and EQ meteorological measurements, we defined dust events as periods with PM₁₀ concentrations
228 exceeding 100 $\mu\text{g}/\text{m}^3$ accompanied by winds exceeding 5 m/s at either site. These high winds were either observed at
229 the beginning or during dust events. Each dust event typically included a period of time when PM₁₀ concentrations
230 began increasing before reaching peak values. After wind speeds began to decrease, PM₁₀ concentration decreased
231 gradually. The dust events in this study included the entire time period when wind/PM₁₀ levels decreased until PM₁₀
232 concentrations reached background levels ($<50 \mu\text{g}/\text{m}^3$). Table 2 (for HW) and Table 1S (for EQ) provide the

233 meteorological parameters (wind speed, wind direction, temperature, and RH), PM_{2.5} and PM₁₀ concentrations, and
 234 PM_{2.5}/PM₁₀ ratios for each event.

235

236 We performed a linear regression to relate the PM₁₀ concentration measurements of the low-cost sensors to reference
 237 monitors at HW and EQ and a research monitor at the RS. Performance guidelines for low-cost PM₁₀ measurements
 238 are not yet available. For discussion purposes, we use EPA guidelines for low-cost PM_{2.5} sensors, which include
 239 acceptable performance as a slope of 1 ± 0.35 , intercept of $0 \pm 5 \mu\text{g}/\text{m}^3$, root mean square error (RMSE) $\leq 7 \mu\text{g}/\text{m}^3$,
 240 normalized root mean square error (NRMSE) $\leq 30\%$, and $R^2 > 0.7$ (when compared with the reference monitor)
 241 (Rachelle M. Duvall et al., 2021). RMSE and NRMSE were calculated using the following equations:

$$242 \quad RMSE = \sqrt{\frac{1}{N} \sum_{t=1}^N (low\ cost\ sensor_t - Ref_t)^2}$$

$$243 \quad NRMSE = \frac{RMSE}{\overline{Ref}} \times 100$$

244 where, *low cost sensor* represents the low-cost sensor measurement, \overline{Ref} represents the reference/regulatory
 245 measurements, and \overline{Ref} represents the average of the reference or regulatory monitor measurements.

246

247 We also explored a PM_{2.5}/PM₁₀ ratio-based calibration strategy for correcting PMS sensor readings. Based on the ratio
 248 of FEM-HW PM_{2.5}/PM₁₀, we segregated the FEM-HW and PMS-HW PM₁₀ measurements into six bins: PM_{2.5}/PM₁₀:
 249 <0.2 , $0.2-0.3$, $0.3-0.4$, $0.4-0.5$, $0.5-0.7$, and >0.7 . For each bin, the co-located PMS-HW PM₁₀ concentrations were
 250 linearly regressed against the FEM-HW PM₁₀ concentrations to obtain correction factors (slope and intercept). These
 251 correction factors were later used to correct the PMS PM₁₀ concentrations at the other two locations (RS and EQ). The
 252 PM_{2.5}/PM₁₀ ratios from the GRIMM and OPC-RS at the RS were calculated for use in the in selecting the appropriate
 253 PM-ratio-based correction factor and subsequent correction of the collocated PMS sensors. At the EQ site, the
 254 PM_{2.5}/PM₁₀ ratio from the FEM-EQ was used to select the appropriate PM-ratio-based correction factor and
 255 subsequent correction of the nearby PMS sensors.

256

257 **Table 2:** Meteorological and PM characteristics during the non-dust and dust events at the HW monitoring site. The number in the
 258 parenthesis represents the minimum and maximum of the parameter. Parameters for the EQ site can be found in Table S1
 259 (supplementary material).

Start	Duration (hr)	Wind Speed (m/s)	Relative humidity %	Temperature (°C)	PM _{2.5} /PM ₁₀	PM ₁₀ ($\mu\text{g}/\text{m}^3$)
All non-dust duration	658	1.93 [0.26, 6.07]	39.7 [9, 92]	9.58 [-2.78, 23.3]	0.47 [0.056, 1]	165.47 [1.9, 99 [#]]
4/9/22 5:00 AM	7	3.13 [1.13, 4.16]*	37.9 [28, 46]	10.4 [8.3, 13.8]	0.14 [0.10, 0.27]	81.3 [36, 140]

4/11/22 10:00 AM	9	4.12 [2.11, 5.91]	20.9 [12, 37]	12.4 [7.2, 15.6]	0.2 [0.13, 0.36]	67.6 [44, 101]
4/19/22 9:00 AM	10	3.75 [1.64, 5.60]	23.4 [17,32]	16.7 [13.3, 18.3]	0.24 [0.13, 0.36]	96.5 [54, 161]
4/21/22 11:00 AM	23	3.54 [1.02, 6.73]	37.6 [10, 79]	15.6 [7.2,23.9]	0.15 [0.08, 0.24]	141 [51, 274]
4/28/22 9:00 PM	4	3.17 [1.54, 5.14]	36.5 [28, 45]	14.4 [11.1, 17.2]	0.2 [0.10, 0.38]	79.5 [26, 128]

260 #a single measurement with high PM₁₀ concentration (99 µg/m³) was observed at 4/5/2022 12:00 am. The measurement
261 did not meet the dust event criteria and hence was not included in the dust events.

262 *a wind speed of 6.27 m/s was observed at the EQ site.

263

264

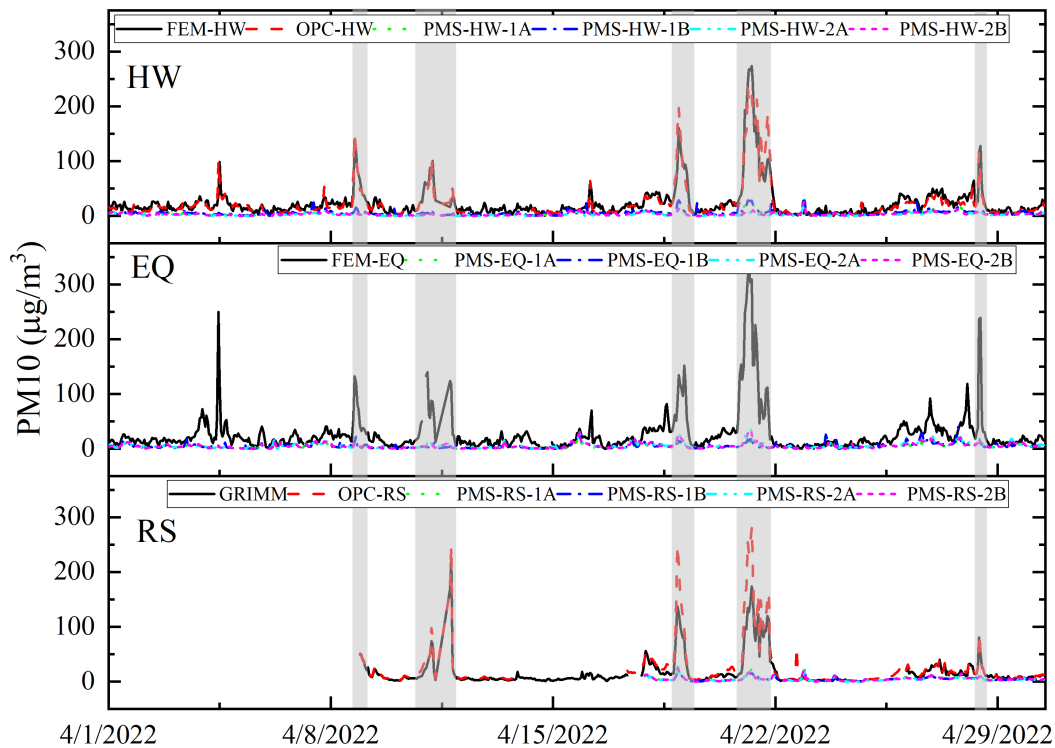
265 3 Results and Discussion

266 Figure 2 shows the hourly average PM₁₀ concentration at the three different sites, with the dust events highlighted in
267 grey. The five dust events were observed at all three locations, and they occurred at approximately the same time.
268 Four of the dust events lasted less than 10 hours, and the event on 21 April 2022 lasted 23 hours. The PM_{2.5}/PM₁₀ ratio
269 (Table 1) remained less than 0.3 during all the events, indicating the predominant contribution of coarser particles to
270 PM₁₀. For each event, the PM₁₀ concentrations reached at least 100 µg/m³. During the 21st April event, hourly average
271 PM₁₀ concentrations reached 275 µg/m³ at HW, 311 µg/m³ at EQ, and 173 µg/m³ at the RS site (Table 1 and Table
272 1S). The lower PM₁₀ concentration at the RS may be due to its residential location, its higher altitude, and its greater
273 distance from dust sources. The OPC-HW and OPC-RS PM₁₀ concentration estimates followed the temporal pattern
274 of the reference/research monitors including during the dust events. Previous studies have observed similar response
275 for OPC-N3 and OPC-N2 (previous version of the OPC-N3) for dust events (Masic et al., 2020; Vogt et al., 2021).
276 Vogt et al. (2021) found that the OPC-N3 tracked PM₁₀ concentrations from a FIDAS (EN 16450 approved regulatory
277 instrument) for long-range transport dust events (PM₁₀ range 60 – 125 µg/m³). The PMS sensors followed the temporal
278 pattern of the reference/research monitors except during the dust events when the PMS sensors substantially
279 underestimated PM₁₀ concentration (Fig. 2). Vogt et al. (2021) also found that the PMS5003 underestimated the PM₁₀
280 concentration during dust events. In addition, Masic et al. (2020) reported that during the Aralkum Desert dust event
281 (PM₁₀ reached 160 µg/m³), the PM₁₀ reported by OPC-N2 agreed well with the GRIMM 11-D (research-grade optical
282 particle sizer), whereas the PMS5003 was not able to detect a large fraction of coarse particles correctly. Most of these
283 studies recorded one dust event during their sampling duration, whereas this study found that the OPC-N3 tracked
284 multiple dust events.

285

286 Figure 3 shows wind roses for April 2022 and each of the dust events. During the month of April, winds exceeding 5
287 m/s were observed at HW during 2.5% of the hours (1.81 % south predominant and 0.69% west predominant). For

288 dust events observed on 11th April and 21-22nd April, the high winds came from the south, whereas, for the rest of the
 289 events, high winds predominantly came from the west. The different wind directions could be transporting dust from
 290 different sources, such as the playas to the south and west of the Salt Lake Valley, the exposed playas of the Great
 291 Salt Lake, or local sources, such as mine tailing, gravel operations, unpaved roads, and an open-pit copper mine
 292 (Hahnenberger and Nicoll, 2012; Perry et al., 2019). All study monitoring sites are located west and southwest of the
 293 Great Salt Lake (Perry et al., 2019). Identifying the sources of the wind-blown dust and the effects of these differences
 294 on sensor performance would require a thorough analysis of the meteorology, the PM composition, and size
 295 distribution during the study period.



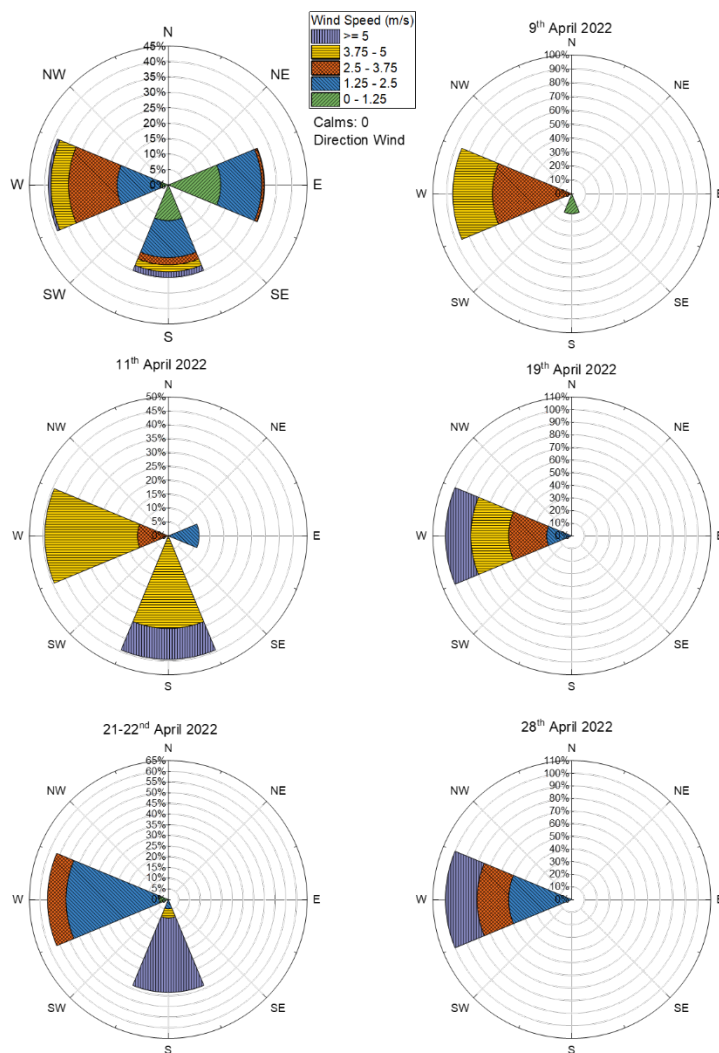
296 **Figure 2:** Hourly averaged PM₁₀ concentrations from the FEM, research monitors and low-cost sensors at the three different sites:
 297 HW, EQ, and RS. Black solid lines represent reference/research monitors; red dash represents OPC-N3; green dot, blue dash-dot,
 298 turquoise dash-dot-dot, and pink short-dash represent PMS sensors. The shaded peaks on 4/9/2022, 4/11/2022, 4/19/2022,
 299 4/21/2022, and 4/28/2022 correspond to dust events. More details on these events can be found in Table 2.
 300

301

302 3.1 OPC-N3 performance

303 Figure 4 illustrates the strong correlation between the OPC-N3 and the PM₁₀ concentration measured by the FEM at
 304 the HW site and the GRIMM monitor at the RS where the coefficient of determination ranges from 0.865 and 0.937.
 305 The intercept, slope, and R² were within the guidelines suggested by the EPA for low-cost PM_{2.5} sensors, although the
 306 RMSE and NRMSE (uncorrected measurements) exceeded the guidelines, 12.4 µg/m³ and 53.5 %, respectively (Fig.

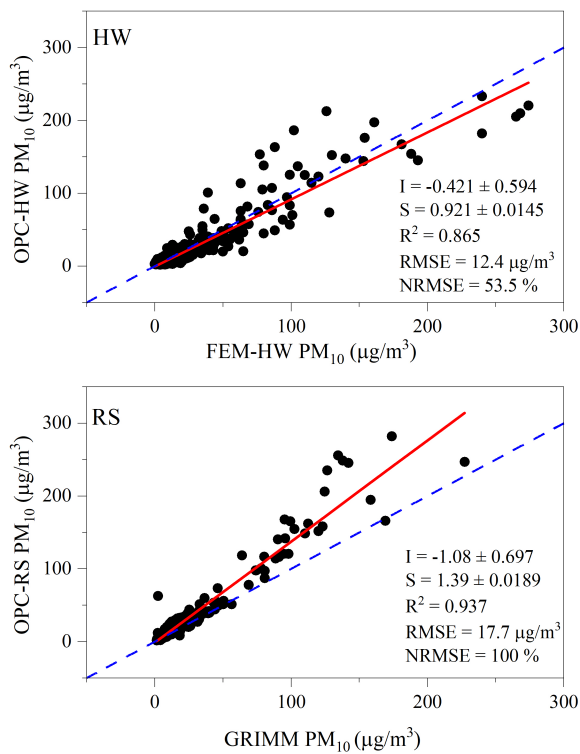
307 4). Vogt et al. (2021) also observed a similar slope (0.84-0.9 $\mu\text{g}/\text{m}^3$) and RMSE (12-13 $\mu\text{g}/\text{m}^3$) for OPC-N3 hourly
308 PM_{10} compared to FIDAS, but with a lower correlation (R^2 0.58-0.64) and for lower concentrations than this study.
309 Vogt et al. (2021) did not correct the PM_{10} measurements for relative humidity, and approximately 20—30% of their
310 measurements corresponded to high humidity conditions ($\text{RH} > 85\%$), and the inclusion of elevated RH conditions
311 may have affected their correlations. The coefficient of determination in this study dropped to 0.81 after the inclusion
312 of measurements corresponding to RH above 85%, which corresponded to just 2% of the total measurements (Fig.
313 S1). Mukherjee et al. (2017) also reported correlations as high as 0.81 for OPC-N2 compared to BAM PM_{10}
314 measurements in the Cuyama Valley of California, with OPC-N2 reporting PM_{10} concentrations of as high as 750
315 $\mu\text{g}/\text{m}^3$. Mukherjee et al. (2017) also did not correct the OPC data for relative humidity, which may have affected their
316 correlations. Our study as well as previous studies suggest that the OPC-N3/OPC-N2 tends to underestimate the PM_{10}
317 concentrations compared to the BAM (Mukherjee et al., 2017; Imami et al., 2022). The operating principle of the
318 BAM and OPC-N3 differ. The BAM PM_{10} measurements are based on beta attenuation and do not require assumptions
319 about particle properties or particle size distribution. In contrast, OPCs rely on the measured particle size distribution
320 and assumed or measured particle properties (i.e., refractive index, shape, and density that can be size dependent) to
321 estimate mass concentration. In addition, particles $< 0.3 \mu\text{m}$ in diameter do not scatter light sufficiently. Consequently,
322 some deviation from the mass measured by the FEM is expected. The assumptions about refractive index and shape
323 affect how particles are size classified, and in addition assumptions about density, affect estimates of mass
324 concentration.



325
 326 **Figure 3:** Wind roses for April 2022 and individual dust events, observed at HW. The wind roses for the EQ site can be found in
 327 the supplementary material (Fig. S13).

328
 329 At the RS site, the OPC-RS showed a strong correlation with the GRIMM ($R^2 > 0.9$) and somewhat overestimated the
 330 PM_{10} concentration (slope = 1.45) compared to the GRIMM's default settings (Fig. 4). Such behavior from OPC-N3
 331 and its predecessor model OPC-N2 has been observed previously. Crilley et al. (2018) also observed this same
 332 behavior for PM_{10} for the OPC-N2 versus the GRIMM (1.108) and reported that the OPC-N2 estimated two to five
 333 times greater PM_{10} mass than the GRIMM. Sousan et al. (2016) observed a slope of 1.6 for the Alphasense OPC-N2
 334 compared to a GRIMM (1.108) for Arizona Road Dust. They attributed this behavior to the higher detection efficiency
 335 of OPC-N2 for particles $> 0.8 \mu m$ compared to the GRIMM, and the effect of aerosol composition on OPC-N2
 336 readings. Unlike Sousan et al. (2016), Bezantakos et al. (2018), using polystyrene spheres (size: 0.8, 1, 2.5, 5.1, 7.2,
 337 and $10.2 \mu m$), reported that the OPC-N2 overestimated particle number concentrations, compared to GRIMM (1.109),
 338 for all sizes, not just size $> 1 \mu m$.

339 Crilley et al.(2018) considered high relative humidity as a controlling factor behind the overestimation by the OPC-
 340 N2. Badura et al. (2018) also reported a strong effect of relative humidity on the OPC-N2 measurements. We excluded
 341 measurement corresponding to $RH > 85\%$ because we focus on dust events, and RH is low during these events. We
 342 investigated the effect of RH (after excluding values $> 85\%$) by performing a multilinear regression with the FEM-
 343 HW as the dependent variable and the OPC-HW PM_{10} concentration and RH as independent variables. Adding RH
 344 did not significantly improve the correlation coefficient (not including RH: $R^2 = 0.865$, $RMSE = 12 \mu g/m^3$; including
 345 RH: $R^2 = 0.872$, $RMSE = 11.7 \mu g/m^3$; Section S1, Supplementary material). Hygroscopic growth changes with PM
 346 composition (Masic et al. 2020), and correcting measurements using a constant humidity coefficient can inject noise
 347 into the results. In addition, the Salt Lake Valley is in an arid region, and 82% of PM measurements corresponded to
 348 an RH of less than 60%. Consequently, the measurements were not corrected for the relative humidity for this study.



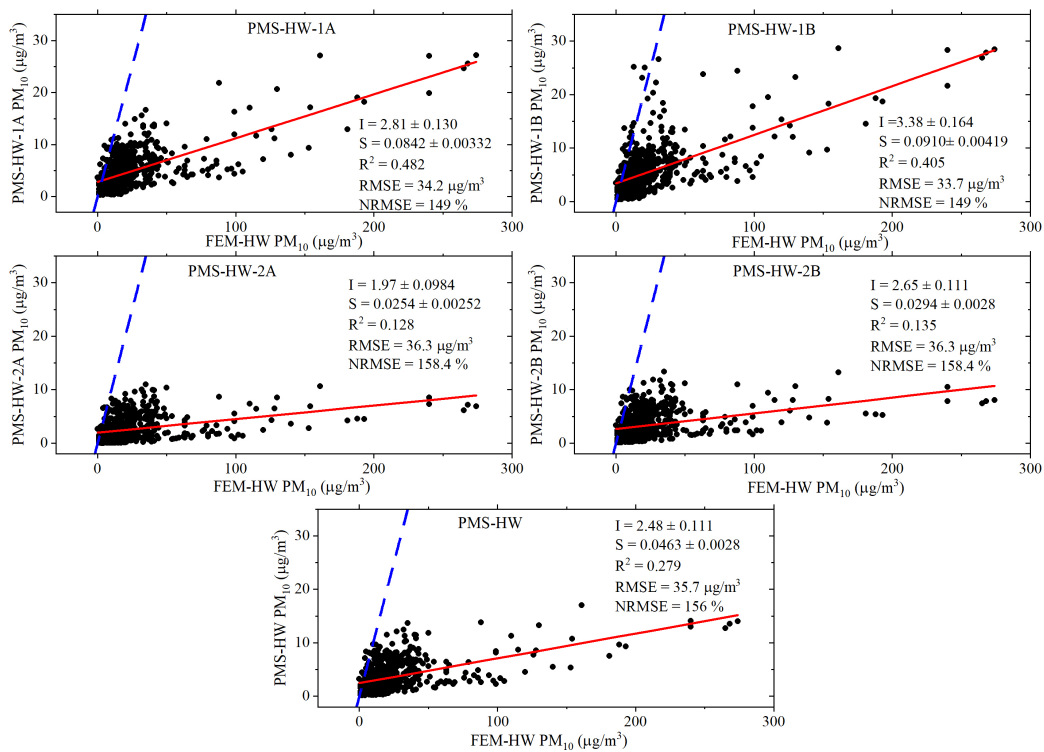
349
 350 **Figure 4:** Hourly averaged PM_{10} concentration (top) OPC-HW vs. FEM-HW PM_{10} concentration for the period between 04/1/2022-
 351 04/30/2022, (bottom) OPC-RS vs. GRIMM PM_{10} concentration at the RS for the sampling period 04/09/2022-04/30/2022. The red
 352 solid line represents linear fit, and the blue dashed line represents the 1:1 line. I: intercept; S: slope.

353

354 3.2 Performance of the PMS5003

355 Figure 5, Figure 7 (top), and Figure 8 (top) illustrate the PMS sensors' poor-to-moderate correlations (R^2 between
 356 0.128 and 0.482) with reference/research measurements of PM_{10} concentration; these sensors underestimate the PM_{10}
 357 concentration (slope < 0.09), particularly during dust events. These sensors also show high RMSEs ($> 30 \mu g/m^3$). Poor
 358 performance of PMS sensors for PM_{10} has been reported previously (Masic et al., 2020; Sayahi et al., 2019). Unlike

359 the OPC-N3, PMS sensors are nephelometers (Ouimette et al., 2022) and not optical particle counters, and their
 360 response decreases with increasing size. Previous studies reported decreased response from PMS 5003 sensors for
 361 particles larger than 0.5 μm (He et al., 2020; Kuula et al., 2020; Tryner et al., 2020). Kuula et al. (2020) and Tryner et
 362 al. (2020) observed constant particle size distributions from the PMS 5003 regardless of actual particle size (exposed
 363 monodisperse particles from polystyrene latex spheres, 0.1 – 2 μm , or generated with di-octyl sebacate 0.5– 10 μm).
 364 The PMS sensors' inability to aspirate particles larger 2.5 μm is a significant cause of these sensors' inability to detect
 365 coarse particles (aerodynamic size between 2.5 – 10 μm), such as those that dominate dust events (Ouimette et al.
 366 2021).
 367



368
 369 **Figure 5:** PMS PM₁₀ concentration vs. FEM-HW PM₁₀ concentration. PMS-HW represents the average of three PMS sensors
 370 (PMS-HW-1A, PMS-HW-2A, and PMS-HW-2B). The red solid line represents linear fit, and the blue line represents the 1:1 line.
 371 The plot includes measurements recorded between 04/1/2022 – 04/30/2022. I: intercept, and S: slope. Each measurement represents
 372 hourly averaged PM₁₀ concentrations.

373
 374 The PMS sensors also exhibited some inter-sensor variability during this study (Fig. S2). One sensor, PMS-HW-1B,
 375 exhibited a fair correlation with the other three PMS sensors ($R^2 = 0.53$ - 0.55 with slopes differing by more than 50%).
 376 The remaining three sensors (when compared to each other) had R^2 greater than 0.7, although their slopes differed by
 377 40% (slope: PMS-HW-2A vs. PMS-HW-1A = 0.504; PMS-HW-2B vs PMS-HW-1A = 0.577). In terms of response

378 to PM_{10} and correlation with the reference monitor, PMS-HW-1(A and B) performed somewhat better than PMS-HW-
379 2 (A and B) ($RMSE < 35 \mu g/m^3$ and $R^2 > 0.4$, compared to $RMSE < 36$ and $R^2 > 0.15$).

380
381 Sensor-to-sensor variability has been reported in previous studies of PMS sensors, particularly for $PM_{2.5}$ concentration
382 (Sayahi et al., 2019; Tagle et al., 2020). The two PurpleAir II sensors (four PMS sensors) at the HW site were deployed
383 on different dates. PMS-HW-1 was deployed on 4/24/2020, whereas the PMS-HW-2 was deployed on 9/20/2019.
384 These sensors could be from different manufacturing batches, and they experienced different amounts of time in the
385 field. Sensor aging can cause differences in PMS sensor performance (Tryner et al., 2020). In addition, because the
386 PMS sensors are inefficient at measuring particles larger than $PM_{2.5} \mu m$ in diameter, as evidenced by the low slopes
387 in Figure 5, small differences (potentially due to sensor orientation and inherent differences in the sensors themselves)
388 can magnify sensor to sensor variability. Mukherjee et al. (2017) and Duvall et al. (2021) discuss the importance of
389 sampler positioning for PM_{10} measurements. For presentation purposes, we have excluded the PMS-HW-1B, which
390 exhibited poor correlation with the other PMS sensors (PMS-HW-1A, PMS-HW-2A, and PMS-HW-2B), and
391 averaged the remaining three PMS PM_{10} concentrations at HW and compared the average of the three sensors to the
392 PM_{10} concentrations measured by the FEM. Figure 5 shows the poor R^2 between the average of all PMS sensors and
393 FEM PM_{10} ($R^2 = 0.279$), and how the PMS-HW underestimates the PM_{10} composition (slope of 0.0463).

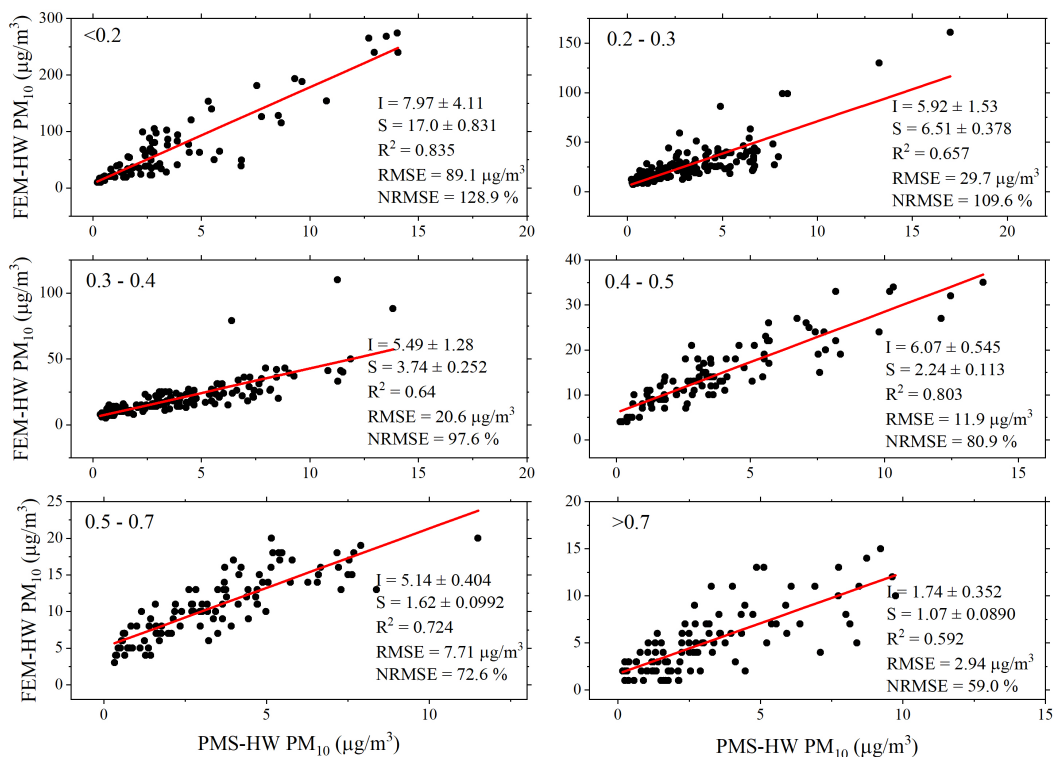
394

395 **3.3 Using $PM_{2.5}/PM_{10}$ ratios to obtain size-segregated PMS correction factors**

396 The effect of correcting the PMS measurements with $PM_{2.5}/PM_{10}$ ratio-based factors on PMS performance was
397 explored as a strategy to obtain correction factors that could enable the PMS measurements to infer PM_{10}
398 concentrations. The $PM_{2.5}/PM_{10}$ ratio, calculated using the $PM_{2.5}$ and PM_{10} concentrations reported by the FEM-HW,
399 was used to segregate the PMS-HW measurements into six bins: $PM_{2.5}/PM_{10}$: <0.2 , $0.2-0.3$, $0.3-0.4$, $0.4-0.5$, $0.5-0.7$,
400 >0.7 . For all the binned ratios (Figure 6), the PMS showed a consistent R^2 of greater than 0.6 (compared to R^2 values
401 of $0.128 - 0.482$ prior to binning), but with very different slopes for the different $PM_{2.5}/PM_{10}$ bins. The slope varied
402 between $17 - 1.07$, with the magnitude decreasing with the $PM_{2.5}/PM_{10}$ ratio. Note that Figures 4 and 5 show the FEM
403 on the x axes, whereas Figure 6 shows the regression equations used for correcting the PMS measurements (with FEM
404 on the y axes). During the dust events, the $PM_{2.5}/PM_{10}$ ratio was less than 0.3, supporting the large contribution from
405 dust and the corresponding large magnitude of PM_{10} concentration. The PM_{10} concentrations were lowest for the high
406 $PM_{2.5}/PM_{10}$ ratios (>0.7), and most PM_{10} concentrations were below $5 \mu g/m^3$, which is close to the BAM's lower limit
407 of detection (Met One Technical Bulletin BAM-1020 Detection Limit, 2022) and likely contributes to the low
408 correlation observed for this ratio.

409

410 The slope and intercept for each bin were used as correction factors, called PM-ratio-based correction factors, to
411 correct the PMS PM_{10} measurements at the other two locations, i.e., RS and EQ.



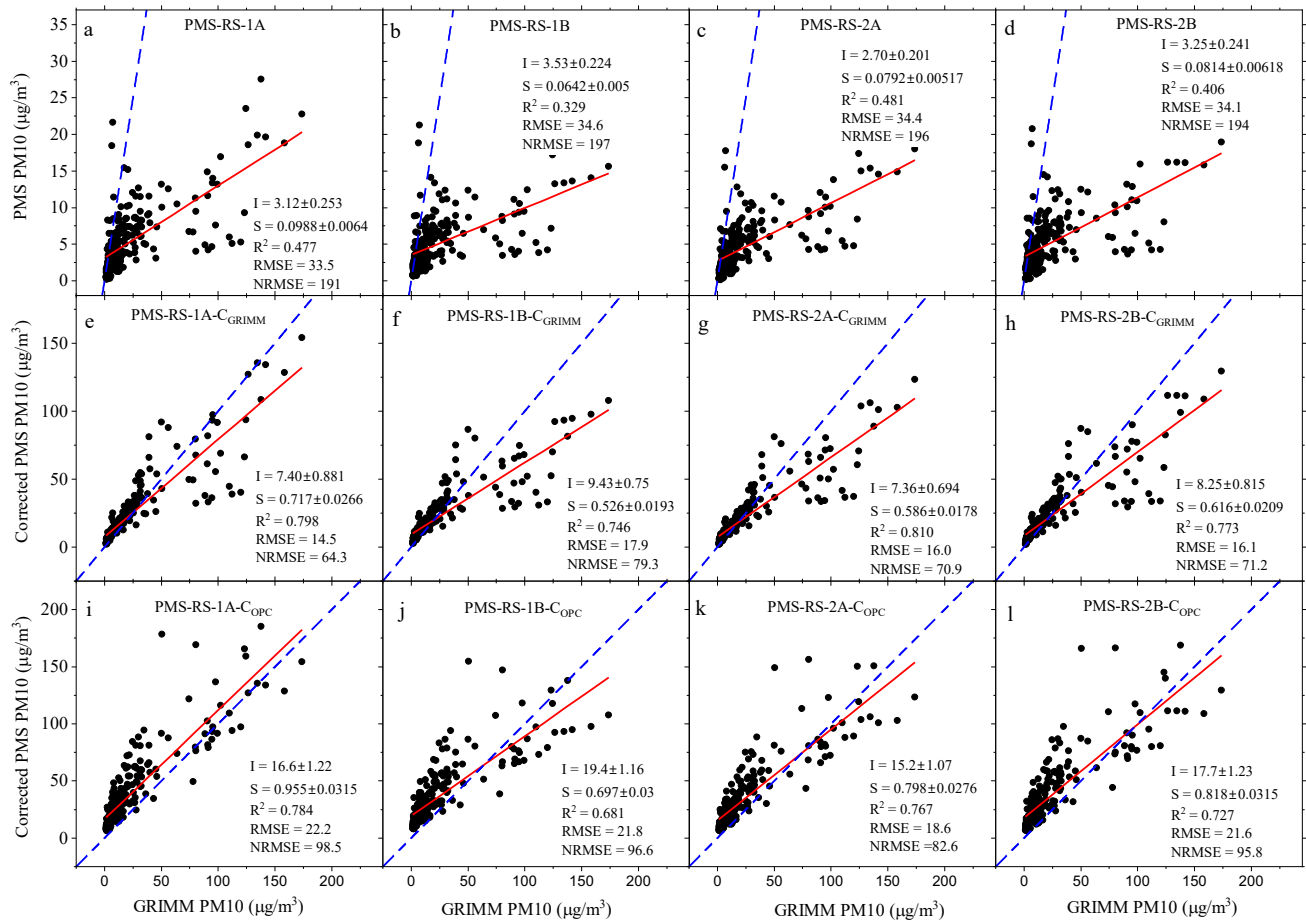
412 **Figure 6:** PMS-HW PM₁₀ concentration (average of three PMS sensors at HW) vs. FEM-HW PM₁₀ concentration for different
 413 PM_{2.5}/PM₁₀ bins. The RMSE and NRMSE has units μg/m³ and %, respectively. Each measurement represents hourly averaged PM₁₀
 414 concentrations.
 415

416
 417

418 3.4 Correcting PMS data at RS and EQ sites

419 Similar to the HW site, the PMS PM₁₀ concentration measurements at the RS (Fig. 7, top) exhibited poor-to-moderate
 420 correlation (R² between 0.32-0.49, RMSE > 33 μg/m³) compared to the research monitor and underestimated the PM₁₀
 421 concentrations (slope <0.099). We corrected the raw PMS PM₁₀ concentration measurements using the PM-ratio-
 422 based correction factors obtained from the HW site and the PM_{2.5}/PM₁₀ ratio from the GRIMM or the OPC to select
 423 a correction factor for each of the six PM_{2.5}/PM₁₀ bins. Using the GRIMM provided ratios, Figure 7 (middle) shows
 424 that at the RS, after PM-ratio-based correction of the PM₁₀ measurements, the correlation for all the PMS sensors
 425 improved significantly (R² > 0.77) and the RMSEs decreased (< 18 μg/m³). The R² varied between 0.773-0.810, and
 426 the slopes varied between 0.526-0.717. The intercept was a little higher (7-10 μg/m³) than the EPA suggested guideline
 427 for low-cost PM_{2.5} sensors. All the PMS sensors at RS were freshly deployed and were all mounted on the east side
 428 of a small building. These sensors exhibited good inter-sensor correlation (Fig. S4, R² > 0.97, slope > 0.77) and
 429 therefore exhibited very similar improvement all the sensors using the PM-ratio-based correction. The correlations
 430 between PMS PM₁₀ and GRIMM PM₁₀ concentrations were also good (R² > 0.7) when considering PM₁₀ < 50 μg/m³

431 (Fig. S8 vs. Fig. S9), indicating that PM-ratio-based correction factors are applicable during more typical ambient
 432 levels of PM₁₀ (without dust events).
 433



434
 435

436 **Figure 7:** (Top: a, b, c, and d) Uncorrected PMS PM₁₀ concentration vs. GRIMM PM₁₀ concentration at RS the site. (Middle: e, f,
 437 g, and h) Corrected PM₁₀ concentrations using the PM-ratio-based correction factors developed at HW and the PM_{2.5}/PM₁₀ ratios
 438 provided by the GRIMM at the RS. (Bottom: i, j, k, and l) Corrected PM₁₀ concentrations using the PM-ratio-based correction
 439 factors developed at HW and the PM_{2.5}/PM₁₀ ratios provided by the OPC-RS at the RS. The solid red line represents the linear fit
 440 and the blue dash line represents the 1:1 line. The plots include measurements recorded between 04/18/2022 – 04/30/2022. I:
 441 intercept; S: slope. The RMSE and NRMSE has units μg/m³ and %, respectively. Each measurement represents hourly averaged
 442 PM₁₀ concentrations.

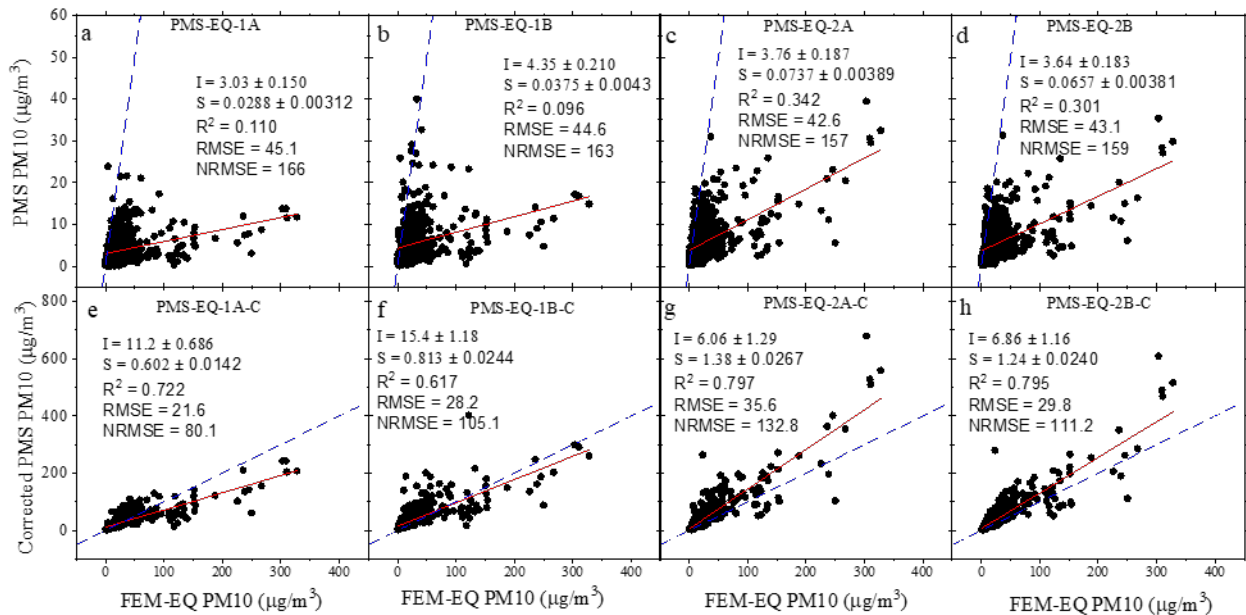
443

444 Figure 7 (bottom) illustrates a similar strategy at the RS site but using the OPC-RS to provide the PM_{2.5}/PM₁₀ ratio. It
 445 also shows that the correlation for PMS sensors improved after applying the PM-ratio-based correction using the OPC-
 446 RS for the ratio (R² = 0.681 - 0.784). After correction, the slope also increased and varied between 0.589-0.813. The
 447 corrected RMSE (18.6 – 22.2 μg/m³) and intercept (15.2-19.4 μg/m³) were somewhat higher than that observed when
 448 using GRIMM-reported PM ratios (Fig. 7 (middle)). From Figure 7 (bottom), the PM-ratio-based corrected PMS PM₁₀
 449 concentration for PM₁₀ < 50 μg/m³ was always above the 1:1 line, i.e., the PMS PM₁₀ concentration was overestimated.
 450 The OPC-RS efficiency in counting particles smaller than 0.8 μm is lower than the GRIMM (Bezantakos et al., 2018;

451 Sousan et al., 2016), and therefore underestimates PM_{2.5} mass. Figure S5 also illustrates this overestimation in our
 452 study, where for low PM_{2.5} and PM₁₀ concentrations (90% of the measurements when PM_{2.5} < 12 µg/m³ and PM₁₀ <
 453 40 µg/m³) the OPC-RS underestimated the PM_{2.5} mass compared to the GRIMM, although the OPC-RS PM₁₀
 454 concentrations were similar to those of the GRIMM. The underestimated PM_{2.5} measurements from the OPC affected
 455 the PM_{2.5}/PM₁₀ ratios, which for the OPC-RS remained lower than those reported by the GRIMM (Fig. S6). The
 456 magnitude of the PM-ratio-based correction factors (Fig. 6) was inversely related to the PM_{2.5}/PM₁₀ ratio. Since the
 457 OPC-RS reported ratios were always low, the corrected PM₁₀ measurements below 50 µg/m³ were overestimated (Fig
 458 S10).

459
 460 At the EQ site, we used the PM_{2.5}/PM₁₀ ratios from FEM measurements at the EQ site coupled with the PM-ratio-
 461 based correction factors developed at the HW site to correct the PMS PM₁₀ concentrations from sensors located near
 462 the EQ site. Correcting the PMS PM₁₀ concentrations using this approach did improve the correlation with FEM-EQ
 463 (Fig. 8). Before the correction, all the PMS sensors has poor correlation with the FEM ($R^2 < 0.342$ and slope < 0.0737).
 464 The R^2 improved to 0.617 - 0.797, and the slope increased to 0.602-1.38 after PM-ratio-based correction. The RMSE
 465 decreased and ranged between 21.5 – 35.6 µg/m³. The intercept increased and varied between 6.06-15.4. The sensors
 466 at this site showed moderate inter-sensor correlation (Fig. S7), which was expected as these sensors were not
 467 collocated. The different correlations with respect to FEM-EQ for the two PurpleAir II were also expected as these
 468 sensors were not collocated with the FEM-EQ.

469



470

471

472 **Figure 8:** (top: a, b, c, and d) Uncorrected PMS PM₁₀ concentration vs. FEM-EQ PM₁₀ concentrations at the EQ site. (bottom: e,
 473 f, g, and h) Corrected PM₁₀ concentrations using the correction factors developed at HW and the PM_{2.5}/PM₁₀ ratios calculated using
 474 FEM-EQ PM₁₀ and PM_{2.5} concentrations. The solid red line represents the linear fit and the blue dash line represents the 1:1 line.
 475 The plots include measurements recorded between 04/1/2022 – 04/30/2022. I: intercept; S: slope. The RMSE and NRMSE has
 476 units µg/m³ and %, respectively. Each measurement represents hourly averaged PM₁₀ concentrations.

477 **4 Limitations**

478 This study has several limitations. The sensor's performance was evaluated for a month-long period in April 2022 and
479 focused primarily on dust events, which commonly occur during this month. Understanding the OPC-N3 performance
480 and whether using a $PM_{2.5}/PM_{10}$ ratio-based correction could improve correction factors for PMS sensors in other
481 seasons and under different environmental conditions, like, wildfires, cold air pools, etc., would require a longer period
482 of evaluation. This study used four PMS5003 sensors at the HW site and unlike the RS site, the sensors at HW were
483 deployed at different times. These sensors showed moderate inter-sensor correlation, suggesting the need for further
484 investigation of sensor age, sensor siting for PM_{10} measurements, and potentially recalibration. This study occurred
485 in an arid region, with RH generally less than 60%. This study did not find a significant improvement by adding RH
486 to a calibration model between the OPC-N3 and the FEM. However, this study excluded measurements with a RH >
487 85% (<2% of total measurements), a range where previous studies have identified a significant effect of RH (Crisley
488 et al., 2018), and the applicability of this study's results to other, more humid, regions would need to be evaluated.
489 The correction factors derived in this study used an average of three co-located PMS sensor measurements at a single
490 site. In absence of detailed information about ambient particle properties, this study used default constant density for
491 all the size-bins for OPC-N3. The Alphasense OPC-N3 allows the user to change the size-bin specific density for
492 better estimates of PM_{10} , and if size-bin density and refractive index were available, the OPC measurements could
493 potentially be improved. Our proposed PM-ratio-based calibration method relies on local measurements of the
494 $PM_{2.5}/PM_{10}$ ratio. This requires FEM or other accurate measurements of $PM_{2.5}$ and PM_{10} concentration, and the needed
495 spatial distribution of these accurate $PM_{2.5}$ and PM_{10} concentrations would need to be determined.

497 **5 Conclusions**

498 This study evaluated the performance of Alphasense OPC-N3 PM_{10} measurements compared to FEM and GRIMM
499 measurements during multiple dust events at two locations (HW and RS). The OPC-N3 tracked all the dust events at
500 the two locations and exhibited a strong correlation with reference measurements ($R^2 = 0.865 - 0.937$), RMSE of 12.4-
501 17.7 $\mu\text{g}/\text{m}^3$, and NRMSE of 53.5 - 100 %. Uncorrected PMS5003 PM_{10} measurements showed poor to moderate
502 correlation ($R^2 < 0.49$) with the reference/research monitors at three locations (HW, RS, and EQ), with a RMSE of
503 33-45 $\mu\text{g}/\text{m}^3$ and a NRMSE of 145-197 %. The PMS measurements severely underestimated the PM_{10} concentrations
504 (slope <0.099). We evaluated a PM-ratio-based correction method to improve estimates of PM_{10} concentration from
505 PMS sensors. After applying this method, PMS PM_{10} concentrations correlated reasonably well with FEM
506 measurements ($R^2 > 0.63$) and GRIMM measurements ($R^2 > 0.76$), the RMSE decreased to 15-25 $\mu\text{g}/\text{m}^3$ and NRMSE
507 decreased to 64 - 132 %. Our results suggest that it may be possible to leverage measurements from existing networks
508 relying on low-cost $PM_{2.5}$ sensors to obtain better resolved spatial estimates of PM_{10} concentration using a combination
509 of PMS sensors and measurements of $PM_{2.5}$ and PM_{10} , such as those provided by FEMs, research-grade
510 instrumentation, or the OPC-N3.

511

512 **Data Availability:**

513 The raw and processed data used in the manuscript can be found at: <https://doi.org/10.7278/S50d-xbns-3ge3>

514 **Authors Contribution:**

515 KEK and KK conceptualized the research, collected, and analysed the data. KK developed the original draft and KEK
516 reviewed the original draft. KEK provided the supervision and acquired the funding.

517 **Competing interests:**

518 Dr. Kerry Kelly has a financial interest in the company Tellus Networked Solutions, LCC, which commercializes
519 solutions for environmental monitoring. Their technology was not used as part of this work.

520

521 **Acknowledgements:**

522 This material is based upon work supported by the National Science Foundation under Grant No. 2012091
523 Collaborative Research Network Cluster: Dust in the Critical Zone and under Grant No. 2228600 CIVIC-PG:
524 TRACK A: Community Resilience through Engaging, Actionable, Timely, High-Resolution Air Quality
525 Information (CREATE-AQI). Thanks to PurpleAir for donating two PAIIs to the project.

526 **References:**

- 527 Akinwumiju, A. S., Ajisafe, T., and Adelodun, A. A.: Airborne Particulate Matter Pollution in Akure Metro City,
528 Southwestern Nigeria, West Africa: Attribution and Meteorological Influence, *Journal of Geovisualization and Spatial*
529 *Analysis*, 5, 11, <https://doi.org/10.1007/s41651-021-00079-6>, 2021.
- 530 Alhasa, K., Mohd Nadzir, M., Olalekan, P., Latif, M., Yusup, Y., Iqbal Faruque, M., Ahamad, F., Abd. Hamid, H.,
531 Aiyub, K., Md Ali, S., Khan, M., Abu Samah, A., Yusuff, I., Othman, M., Tengku Hassim, T., and Ezani, N.:
532 Calibration Model of a Low-Cost Air Quality Sensor Using an Adaptive Neuro-Fuzzy Inference System, *Sensors*, 18,
533 4380, <https://doi.org/10.3390/s18124380>, 2018.
- 534 WHO: [https://www.who.int/news-room/fact-sheets/detail/ambient-\(outdoor\)-air-quality-and-health](https://www.who.int/news-room/fact-sheets/detail/ambient-(outdoor)-air-quality-and-health), last access: 5
535 October 2022.
- 536 Ardon-Dryer, K. and Kelley, M. C.: Particle size distribution and particulate matter concentrations during synoptic
537 and convective dust events in West Texas, *Atmos Chem Phys*, 22, 9161–9173, [https://doi.org/10.5194/acp-22-9161-](https://doi.org/10.5194/acp-22-9161-2022)
538 [2022](https://doi.org/10.5194/acp-22-9161-2022), 2022.
- 539 Bächler, P., Szabadi, J., Meyer, J., and Dittler, A.: Simultaneous measurement of spatially resolved particle emissions
540 in a pilot plant scale baghouse filter applying distributed low-cost particulate matter sensors, *J Aerosol Sci*, 150,
541 <https://doi.org/10.1016/j.jaerosci.2020.105644>, 2020.

542 Badura, M., Batog, P., Drzeniecka-Osiadacz, A., and Modzel, P.: Evaluation of low-cost sensors for ambient PM_{2.5}
543 monitoring, *J Sens*, 2018, <https://doi.org/10.1155/2018/5096540>, 2018.

544 Bezantakos, S., Schmidt-Ott, F., and Biskos, G.: Performance evaluation of the cost-effective and lightweight
545 Alphasense optical particle counter for use onboard unmanned aerial vehicles, *Aerosol Science and Technology*, 52,
546 385–392, <https://doi.org/10.1080/02786826.2017.1412394>, 2018.

547 Bi, J., Wildani, A., Chang, H. H., and Liu, Y.: Incorporating Low-Cost Sensor Measurements into High-Resolution
548 PM_{2.5} Modeling at a Large Spatial Scale, *Environ Sci Technol*, 54, 2152–2162,
549 <https://doi.org/10.1021/acs.est.9b06046>, 2020.

550 Bílek, J., Bílek, O., Maršolek, P., and Buček, P.: Ambient air quality measurement with low-cost optical and
551 electrochemical sensors: An evaluation of continuous year-long operation, *Environments - MDPI*, 8,
552 <https://doi.org/10.3390/environments8110114>, 2021.

553 Bogan, M., Al, B., Kul, S., Zengin, S., Oktay, M., Sabak, M., Gümüšboğa, H., and Bayram, H.: The effects of desert
554 dust storms, air pollution, and temperature on morbidity due to spontaneous abortions and toxemia of pregnancy: 5-
555 year analysis, *Int J Biometeorol*, 65, 1733–1739, <https://doi.org/10.1007/s00484-021-02127-8>, 2021.

556 Bousiotis, D., Singh, A., Haugen, M., Beddows, D. C. S., Diez, S., Murphy, K. L., Edwards, P. M., Boies, A., Harrison,
557 R. M., and Pope, F. D.: Assessing the sources of particles at an urban background site using both regulatory
558 instruments and low-cost sensors – a comparative study, *Atmos Meas Tech*, 14, 4139–4155,
559 <https://doi.org/10.5194/amt-14-4139-2021>, 2021.

560 Cai, H., Yang, Y., Luo, W., and Chen, Q.: City-level variations in aerosol optical properties and aerosol type
561 identification derived from long-term MODIS/Aqua observations in the Sichuan Basin, China, *Urban Clim*, 38,
562 100886, <https://doi.org/10.1016/j.uclim.2021.100886>, 2021.

563 Caplin, A., Ghandehari, M., Lim, C., Glimcher, P., and Thurston, G.: Advancing environmental exposure assessment
564 science to benefit society, *Nat Commun*, 10, 1236, <https://doi.org/10.1038/s41467-019-09155-4>, 2019.

565 Caubel, J. J., Cados, T. E., Preble, C. v., and Kirchstetter, T. W.: A Distributed Network of 100 Black Carbon Sensors
566 for 100 Days of Air Quality Monitoring in West Oakland, California, *Environ Sci Technol*, 53, 7564–7573,
567 <https://doi.org/10.1021/acs.est.9b00282>, 2019.

568 Chakravarty, K., Vincent, V., Vellore, R., Srivastava, A. K., Rastogi, A., and Soni, V. K.: Revisiting Andhi in northern
569 India: A case study of severe dust-storm over the urban megacity of New Delhi, *Urban Clim*, 37, 100825,
570 <https://doi.org/10.1016/j.uclim.2021.100825>, 2021.

571 Chu, M. D. T., Gilooly, S. E., Levy, J. I., Vallarino, J., Reyna, L. N., Cedeño Laurent, J. G., Coull, B. A., and
572 Adamkiewicz, G.: Real-time indoor PM_{2.5} monitoring in an urban cohort: Implications for exposure disparities and
573 source control, *Environ Res*, 193, <https://doi.org/10.1016/j.envres.2020.110561>, 2021.

574 Clifford, H. M., Spaulding, N. E., Kurbatov, A. v., More, A., Korotkikh, E. v., Sneed, S. B., Handley, M., Maasch, K.
575 A., Loveluck, C. P., Chaplin, J., McCormick, M., and Mayewski, P. A.: A 2000 Year Saharan Dust Event Proxy
576 Record from an Ice Core in the European Alps, *Journal of Geophysical Research: Atmospheres*, 124, 12882–12900,
577 <https://doi.org/10.1029/2019JD030725>, 2019.

578 Crilley, L. R., Shaw, M., Pound, R., Kramer, L. J., Price, R., Young, S., Lewis, A. C., and Pope, F. D.: Evaluation of
579 a low-cost optical particle counter (Alphasense OPC-N2) for ambient air monitoring, *Atmos Meas Tech*, 11, 709–720,
580 <https://doi.org/10.5194/amt-11-709-2018>, 2018.

581 Dastoorpoor, M., Idani, E., Goudarzi, G., and Khanjani, N.: Acute effects of air pollution on spontaneous abortion,
582 premature delivery, and stillbirth in Ahvaz, Iran: a time-series study, *Environmental Science and Pollution Research*,
583 25, 5447–5458, <https://doi.org/10.1007/s11356-017-0692-9>, 2018.

584 Met One Technical Bulletin BAM-1020 Detection Limit: [https://metone.com/wp-content/uploads/2019/04/bam-
585 1020_detection_limit.pdf](https://metone.com/wp-content/uploads/2019/04/bam-1020_detection_limit.pdf), last access: 5 October 2022.

586 Diokhane, A. M., Jenkins, G. S., Manga, N., Drame, M. S., and Mbodji, B.: Linkages between observed, modeled
587 Saharan dust loading and meningitis in Senegal during 2012 and 2013, *Int J Biometeorol*, 60, 557–575,
588 <https://doi.org/10.1007/s00484-015-1051-5>, 2016.

589 Dubey, R., Patra, A. K., Joshi, J., Blankenberg, D., Kolluru, S. S. R., Madhu, B., and Raval, S.: Evaluation of low-
590 cost particulate matter sensors OPC N2 and PM Nova for aerosol monitoring, *Atmos Pollut Res*, 13,
591 <https://doi.org/10.1016/j.apr.2022.101335>, 2022a.

592 Dubey, R., Patra, A. K., Joshi, J., Blankenberg, D., and Nazneen: Evaluation of vertical and horizontal distribution of
593 particulate matter near an urban roadway using an unmanned aerial vehicle, *Science of the Total Environment*, 836,
594 <https://doi.org/10.1016/j.scitotenv.2022.155600>, 2022b.

595 Duvall, R. M., Hagler, G. S. W., Clements, A. L., Benedict, K., Barkjohn, K., Kilaru, V., Hanley, T., Watkins, N.,
596 Kaufman, A., Kamal, A., Reece, S., Fransioli, P., Gerboles, M., Gillerman, G., Habre, R., Hannigan, M., Ning, Z.,
597 Papapostolou, V., Pope, R., Quintana, P. J. E., and Lam Snyder, J.: Deliberating Performance Targets: Follow-on
598 workshop discussing PM10, NO2, CO, and SO2 air sensor targets, in: *Atmospheric Environment*,
599 <https://doi.org/10.1016/j.atmosenv.2020.118099>, 2021.

600 EPA: <https://www.epa.gov/outdoor-air-quality-data/interactive-map-air-quality-monitors>, last access: 5 October
601 2022.

602 USA EPA: https://aq5.epa.gov/aqsweb/airdata/download_files.html, last access: 4 October 2022.

603 Feenstra, B., Papapostolou, V., Hasheminassab, S., Zhang, H., Boghossian, B. der, Cocker, D., and Polidori, A.:
604 Performance evaluation of twelve low-cost PM2.5 sensors at an ambient air monitoring site, *Atmos Environ*, 216,
605 <https://doi.org/10.1016/j.atmosenv.2019.116946>, 2019.

606 Gomes, J., Esteves, H., and Rente, L.: Influence of an Extreme Saharan Dust Event on the Air Quality of the West
607 Region of Portugal, *Gases*, 2, 74–84, <https://doi.org/10.3390/gases2030005>, 2022.

608 Goudie, A. S.: Desert dust and human health disorders, *Environ Int*, 63, 101–113,
609 <https://doi.org/10.1016/j.envint.2013.10.011>, 2014.

610 Hahnenberger, M. and Nicoll, K.: Meteorological characteristics of dust storm events in the eastern Great Basin of
611 Utah, U.S.A., *Atmos Environ*, 60, 601–612, <https://doi.org/10.1016/J.ATMOSENV.2012.06.029>, 2012.

612 Harr, L., Sinsel, T., Simon, H., Konter, O., Dreiseitl, D., Schulz, P., and Esper, J.: PM2.5 exposure differences between
613 children and adults, *Urban Clim*, 44, <https://doi.org/10.1016/j.uclim.2022.101198>, 2022a.

614 Harr, L., Sinsel, T., Simon, H., and Esper, J.: Seasonal Changes in Urban PM_{2.5} Hotspots and Sources from Low-
615 Cost Sensors, *Atmosphere (Basel)*, 13, <https://doi.org/10.3390/atmos13050694>, 2022b.

616 He, M., Kuerbanjiang, N., and Dhaniyala, S.: Performance characteristics of the low-cost Plantower PMS optical
617 sensor, *Aerosol Science and Technology*, 54, 232–241, <https://doi.org/10.1080/02786826.2019.1696015>, 2020.

618 Huang, J., Ji, M., Xie, Y., Wang, S., He, Y., and Ran, J.: Global semi-arid climate change over last 60 years, *Clim
619 Dyn*, 46, 1131–1150, <https://doi.org/10.1007/s00382-015-2636-8>, 2016.

620 Imami, A. D., Drijeana, Villegas, E. R., and McFiggans, G.: Evaluation of Alphasense OPC-N2 sensor for PM₁₀
621 measurement in the North Jakarta, *ASEAN Engineering Journal*, 12, 243–248,
622 <https://doi.org/10.11113/aej.V12.17853>, 2022.

623 Jayaratne, E. R., Johnson, G. R., McGarry, P., Cheung, H. C., and Morawska, L.: Characteristics of airborne ultrafine
624 and coarse particles during the Australian dust storm of 23 September 2009, *Atmos Environ*, 45, 3996–4001,
625 <https://doi.org/10.1016/j.atmosenv.2011.04.059>, 2011.

626 Jones, B. A.: After the Dust Settles: The Infant Health Impacts of Dust Storms, *J Assoc Environ Resour Econ*, 7,
627 1005–1032, <https://doi.org/10.1086/710242>, 2020.

628 Kaliszewski, M., Włodarski, M., Młyńczak, J., and Kopczyński, K.: Comparison of low-cost particulate matter sensors
629 for indoor air monitoring during covid-19 lockdown, *Sensors (Switzerland)*, 20, 1–17,
630 <https://doi.org/10.3390/s20247290>, 2020.

631 Keet, C. A., Keller, J. P., and Peng, R. D.: Long-Term Coarse Particulate Matter Exposure Is Associated with Asthma
632 among Children in Medicaid, *Am J Respir Crit Care Med*, 197, 737–746, <https://doi.org/10.1164/rccm.201706-1267OC>, 2018.

634 Kelly, K. E., Xing, W. W., Sayahi, T., Mitchell, L., Becnel, T., Gaillardon, P.-E., Meyer, M., and Whitaker, R. T.:
635 Community-Based Measurements Reveal Unseen Differences during Air Pollution Episodes, *Environ Sci Technol*,
636 55, 120–128, <https://doi.org/10.1021/acs.est.0c02341>, 2021.

637 Kosmopoulos, G., Salamalikis, V., Pandis, S. N., Yannopoulos, P., Bloutsos, A. A., and Kazantzidis, A.: Low-cost
638 sensors for measuring airborne particulate matter: Field evaluation and calibration at a South-Eastern European site,
639 *Science of the Total Environment*, 748, <https://doi.org/10.1016/j.scitotenv.2020.141396>, 2020.

640 Kumar, S., Singh, A., Srivastava, A. K., Sahu, S. K., Hooda, R. K., Dumka, U. C., and Pathak, V.: Long-term change
641 in aerosol characteristics over Indo-Gangetic Basin: How significant is the impact of emerging anthropogenic
642 activities?, *Urban Clim*, 38, 100880, <https://doi.org/10.1016/j.uclim.2021.100880>, 2021.

643 Kuula, J., Mäkelä, T., Aurela, M., Teinilä, K., Varjonen, S., González, Ó., and Timonen, H.: Laboratory evaluation of
644 particle-size selectivity of optical low-cost particulate matter sensors, *Atmos Meas Tech*, 13, 2413–2423,
645 <https://doi.org/10.5194/amt-13-2413-2020>, 2020.

646 Lim, C. C., Kim, H., Vilcassim, M. J. R., Thurston, G. D., Gordon, T., Chen, L.-C., Lee, K., Heimbinder, M., and
647 Kim, S.-Y.: Mapping urban air quality using mobile sampling with low-cost sensors and machine learning in Seoul,
648 South Korea, *Environ Int*, 131, 105022, <https://doi.org/10.1016/j.envint.2019.105022>, 2019.

649 Liu, L., Duan, Y., Li, L., Xu, L., Yang, Y., and Cu, X.: Spatiotemporal trends of PM_{2.5} concentrations and typical
650 regional pollutant transport during 2015–2018 in China, *Urban Clim*, 34, 100710,
651 <https://doi.org/10.1016/j.uclim.2020.100710>, 2020.

652 Mallet, M., Tulet, P., Serça, D., Solmon, F., Dubovik, O., Pelon, J., Pont, V., and Thouron, O.: Impact of dust aerosols
653 on the radiative budget, surface heat fluxes, heating rate profiles and convective activity over West Africa during
654 March 2006, *Atmos Chem Phys*, 9, 7143–7160, <https://doi.org/10.5194/acp-9-7143-2009>, 2009.

655 Masic, A., Bibic, D., Pikula, B., Blazevic, A., Huremovic, J., and Zero, S.: Evaluation of optical particulate matter
656 sensors under realistic conditions of strong and mild urban pollution, *Atmos Meas Tech*, 13, 6427–6443,
657 <https://doi.org/10.5194/amt-13-6427-2020>, 2020.

658 Mei, H., Han, P., Wang, Y., Zeng, N., Liu, D., Cai, Q., Deng, Z., Wang, Y., Pan, Y., and Tang, X.: Field evaluation
659 of low-cost particulate matter sensors in Beijing, *Sensors (Switzerland)*, 20, 1–17, <https://doi.org/10.3390/s20164381>,
660 2020.

661 Mohd Nadzir, M. S., Ooi, M. C. G., Alhasa, K. M., Bakar, M. A. A., Mohtar, A. A. A., Nor, M. F. F. M., Latif, M. T.,
662 Hamid, H. H. A., Ali, S. H. M., Ariff, N. M., Anuar, J., Ahamad, F., Azhari, A., Hanif, N. M., Subhi, M. A., Othman,
663 M., and Nor, M. Z. M.: The Impact of Movement Control Order (MCO) during Pandemic COVID-19 on Local Air
664 Quality in an Urban Area of Klang Valley, Malaysia, *Aerosol Air Qual Res*, 20, 1237–1248,
665 <https://doi.org/10.4209/aaqr.2020.04.0163>, 2020.

666 Mukherjee, A., Stanton, L. G., Graham, A. R., and Roberts, P. T.: Assessing the utility of low-cost particulate matter
667 sensors over a 12-week period in the Cuyama valley of California, *Sensors (Switzerland)*, 17,
668 <https://doi.org/10.3390/s17081805>, 2017.

669 Nor, N. S. M., Yip, C. W., Ibrahim, N., Jaafar, M. H., Rashid, Z. Z., Mustafa, N., Hamid, H. H. A., Chandru, K., Latif,
670 M. T., Saw, P. E., Lin, C. Y., Alhasa, K. M., Hashim, J. H., and Nadzir, M. S. M.: Particulate matter (PM_{2.5}) as a
671 potential SARS-CoV-2 carrier, *Sci Rep*, 11, 2508, <https://doi.org/10.1038/s41598-021-81935-9>, 2021.

672 Ouimette, J. R., Malm, W. C., Schichtel, B. A., Sheridan, P. J., Andrews, E., Ogren, J. A., and Arnott, W. P.:
673 Evaluating the PurpleAir monitor as an aerosol light scattering instrument, *Atmos Meas Tech*, 15, 655–676,
674 <https://doi.org/10.5194/amt-15-655-2022>, 2022.

675 Perry, K. D., Crosman, E. T., and Hoch, S. W.: Results of the Great Salt Lake Dust Plume Study (2016–2018), 2019.

676 Pope, F. D., Gatari, M., Ng'ang'a, D., Poynter, A., and Blake, R.: Airborne particulate matter monitoring in Kenya
677 using calibrated low-cost sensors, *Atmos Chem Phys*, 18, 15403–15418, <https://doi.org/10.5194/acp-18-15403-2018>,
678 2018.

679 Rachele M. Duvall, Andrea L. Clements, Gayle Hagler, Ali Kamal, Vasu Kilaru, Laura Goodman, Samuel Frederick,
680 Karoline K. (Johnson) Barkjohn, Ian VonWal, Danny Greene, and Tim Dye: Performance Testing Protocols, Metrics,
681 and Target Values for Fine Particulate Matter Air Sensors: Use in Ambient, Outdoor, Fixed Site, Non-Regulatory
682 Supplemental and Informational Monitoring Applications, 2021.

683 Runström Eden, G., Tinnerberg, H., Rosell, L., Möller, R., Almstrand, A. C., and Bredberg, A.: Exploring Methods
684 for Surveillance of Occupational Exposure from Additive Manufacturing in Four Different Industrial Facilities, *Ann
685 Work Expo Health*, 66, 163–177, <https://doi.org/10.1093/annweh/wxab070>, 2022.

686 Samad, A., Mimiaga, F. E. M., Laquai, B., and Vogt, U.: Investigating a low-cost dryer designed for low-cost PM
687 sensors measuring ambient air quality, *Sensors (Switzerland)*, 21, 1–18, <https://doi.org/10.3390/s21030804>, 2021.

688 Sayahi, T., Butterfield, A., and Kelly, K. E.: Long-term field evaluation of the Plantower PMS low-cost particulate
689 matter sensors, *Environmental Pollution*, 245, 932–940, <https://doi.org/10.1016/j.envpol.2018.11.065>, 2019.

690 Schweitzer, M. D., Calzadilla, A. S., Salamo, O., Sharifi, A., Kumar, N., Holt, G., Campos, M., and Mirsaedi, M.:
691 Lung health in era of climate change and dust storms, *Environ Res*, 163, 36–42,
692 <https://doi.org/10.1016/j.envres.2018.02.001>, 2018.

693 Sousan, S., Koehler, K., Hallett, L., and Peters, T. M.: Evaluation of the Alphasense optical particle counter (OPC-
694 N2) and the Grimm portable aerosol spectrometer (PAS-1.108), *Aerosol Science and Technology*, 50, 1352–1365,
695 <https://doi.org/10.1080/02786826.2016.1232859>, 2016.

696 Sousan, S., Regmi, S., and Park, Y. M.: Laboratory evaluation of low-cost optical particle counters for environmental
697 and occupational exposures, *Sensors*, 21, <https://doi.org/10.3390/s21124146>, 2021.

698 Soy, F. K.: The effects of dust storms on quality of life of allergic patients with or without asthma, *The Turkish Journal*
699 *of Ear Nose and Throat*, 26, 19–27, <https://doi.org/10.5606/kbbihtisas.2016.56254>, 2016.

700 Speranza, A., Caggiano, R., Margiotta, S., and Trippetta, S.: A novel approach to comparing simultaneous size-
701 segregated particulate matter (PM) concentration ratios by means of a dedicated triangular diagram using the Agri
702 Valley PM measurements as an example, *Natural Hazards and Earth System Sciences*, 14, 2727–2733,
703 <https://doi.org/10.5194/nhess-14-2727-2014>, 2014.

704 Sugimoto, N., Shimizu, A., Matsui, I., and Nishikawa, M.: A method for estimating the fraction of mineral dust in
705 particulate matter using PM_{2.5}-to-PM₁₀ ratios, *Particuology*, 28, 114–120,
706 <https://doi.org/10.1016/j.partic.2015.09.005>, 2016.

707 Tagle, M., Rojas, F., Reyes, F., Vásquez, Y., Hallgren, F., Lindén, J., Kolev, D., Watne, Å. K., and Oyola, P.: Field
708 performance of a low-cost sensor in the monitoring of particulate matter in Santiago, Chile, *Environ Monit Assess*,
709 192, 171, <https://doi.org/10.1007/s10661-020-8118-4>, 2020.

710 Tam, W. W. S., Wong, T. W., Wong, A. H. S., and Hui, D. S. C.: Effect of dust storm events on daily emergency
711 admissions for respiratory diseases, *Respirology*, 17, 143–148, <https://doi.org/10.1111/j.1440-1843.2011.02056.x>,
712 2012.

713 Alphasense Ltd: <https://www.alphasense.com/wp-content/uploads/2022/09/Alphasense OPC-N3 datasheet.pdf>, last
714 access: 12 October 2022.

715 Tong, D. Q., Wang, J. X. L., Gill, T. E., Lei, H., and Wang, B.: Intensified dust storm activity and Valley fever
716 infection in the southwestern United States, *Geophys Res Lett*, 44, 4304–4312,
717 <https://doi.org/10.1002/2017GL073524>, 2017.

718 Trianti, S.-M., Samoli, E., Rodopoulou, S., Katsouyanni, K., Papiris, S. A., and Karakatsani, A.: Desert dust outbreaks
719 and respiratory morbidity in Athens, Greece, *Environmental Health*, 16, 72, [https://doi.org/10.1186/s12940-017-0281-](https://doi.org/10.1186/s12940-017-0281-x)
720 [x](https://doi.org/10.1186/s12940-017-0281-x), 2017.

721 Tryner, J., Mehaffy, J., Miller-Lionberg, D., and Volckens, J.: Effects of aerosol type and simulated aging on
722 performance of low-cost PM sensors, *J Aerosol Sci*, 150, 105654, <https://doi.org/10.1016/j.jaerosci.2020.105654>,
723 2020.

724 Vogt, M., Schneider, P., Castell, N., and Hamer, P.: Assessment of low-cost particulate matter sensor systems against
725 optical and gravimetric methods in a field co-location in norway, *Atmosphere (Basel)*, 12,
726 <https://doi.org/10.3390/atmos12080961>, 2021.

727 Williams, A. P., Cook, B. I., and Smerdon, J. E.: Rapid intensification of the emerging southwestern North American
728 megadrought in 2020–2021, *Nat Clim Chang*, 12, 232–234, <https://doi.org/10.1038/s41558-022-01290-z>, 2022.

729 Xu, G., Jiao, L., Zhang, B., Zhao, S., Yuan, M., Gu, Y., Liu, J., and Tang, X.: Spatial and temporal variability of the
730 PM_{2.5}/PM₁₀ ratio in Wuhan, Central China, *Aerosol Air Qual Res*, 17, 741–751,
731 <https://doi.org/10.4209/aaqr.2016.09.0406>, 2017.

732